hedral angle between the O-Zr-Cl planes of $[X(C_5H_4)_2][(C_5H_5)ZrCl]_2(\mu\text{-}O)$ is more or less set at ca. 45°. Further, the distance between the ring centroids of the bridged cyclopentadienyl rings affects the Zr-O-Zr bond angle by altering the directional properties of the acceptor orbitals involved in oxo-bridge formation. A decrease in this distance from 4.95 (1) Å in $[SiMe_2(C_5H_4)_2][(C_5H_5)ZrCl]_2(\mu\text{-}O)$ to 4.82 (1) Å[31] in $[CH_2(C_5H_4)_2][(C_5H_5)ZrCl]_2(\mu\text{-}O)$ to 3.84 Å (estimated) in $(C_{10}H_8)[(C_5H_5)ZrCl]_2(\mu\text{-}O)$[8q] is accompanied by a parallel reduction in the Zr-O-Zr bond angle from 178.6 (2)° to 174.3 (2)° to 156.0 (2)°, respectively. Consequently, the size/length of the bridging linkage exhibits a significant influence on the central geometry of these modified oxo-bridged zirconocene complexes.

In summary, convenient synthetic procedures have been developed for the preparation of a new class of binuclear zirconocenophane complexes. The availability of $[X(C_5H_4)_2][(C_5R_5)ZrCl_2]_2$ and $[X(C_5H_4)_2][(C_5H_5)ZrCl]_2(\mu\text{-}O)$ has provided appropriate starting materials for synthesizing other binuclear derivatives, including $[SiMe_2(C_5H_4)_2][(C_5H_5)ZrL(\mu\text{-}H)]_2$ (L = H, Cl) and $[SiMe_2(C_5H_4)_2][(C_5H_5)Zr(\mu\text{-}Cl)]_2$.[32] Current efforts are directed at exploring the potential cooperative chemical effects introduced by the near proximity of two high-valent zirconium centers in these zirconocenophane complexes.

Acknowledgment. Support for this research was provided by the West Virginia Energy and Water Research Center. Computer time for the X-ray structural analyses was provided by the West Virginia Network for Educational Telecomputing.

Registry No. CH_2Br_2, 74-95-3; $SiMe_2Cl_2$, 75-78-5; $CH_2(C_5H_5)_2$, 79249-50-6; $SiMe_2(C_5H_5)_2$, 18053-74-2; $Li_2[CH_2(C_5H_4)_2]$, 121706-37-4; $Li_2[SiMe_2(C_5H_4)_2]$, 87122-68-7; $(C_5H_5)ZrCl_3$, 34767-44-7; $(C_5Me_5)ZrCl_3$, 75181-07-6; $[SiMe_2(C_5H_4)_2][(C_5Me_5)ZrCl_2]_2$, 121730-60-7; $[SiMe_2(C_5H_4)_2][(C_5H_5)ZrCl_2]_2$, 118920-56-2; $[CH_2(C_5H_4)_2][(C_5Me_5)ZrCl_2]_2$, 121730-61-8; $[CH_2(C_5H_4)_2][(C_5H_5)ZrCl_2]_2$, 121730-62-9; $[SiMe_2(C_5H_4)_2[(C_5H_5)ZrCl]_2(\mu\text{-}O)$, 118920-57-3; $[CH_2(C_5H_4)_2][(C_5H_5)ZrCl]_2(\mu\text{-}O)$, 121730-63-0; $[SiMe_2(C_5H_4)_2][(C_5Me_5)ZrCl_2]_2 \cdot {}^1/_2C_7H_8$, 121754-77-6; $[CH_2(C_5H_4)_2][(C_5H_5)ZrCl]_2(\mu\text{-}O)\cdot C_6H_6$, 121730-64-1.

Supplementary Material Available: Tables of positional and thermal parameters, interatomic distances and bond angles, and least-squares planes for the X-ray structural analyses of $[SiMe_2(C_5H_4)_2][(C_5Me_5)ZrCl_2]_2 \cdot {}^1/_2C_7H_8$ and $[SiMe_2(C_5H_4)_2][(C_5H_5)ZrCl]_2(\mu\text{-}O)$ and a table of the refined positional and thermal parameters for the X-ray structure determination of $[CH_2(C_5H_4)_2][(C_5H_5)ZrCl]_2(\mu\text{-}O)\cdot C_6H_6$ (31 pages); listings of observed and calculated structure factors (34 pages). Ordering information is given on any current masthead page.

(31) Crystal data for $[CH_2(C_5H_4)_2][(C_5H_5)ZrCl]_2(\mu\text{-}O)\cdot C_6H_6$: space group $P\bar{1}$, a = 11.891 (4) Å, b = 12.736 (5) Å, c = 13.129 (6) Å, α = 114.02 (3)°, β = 115.34 (2)°, γ = 111.39 (3)°, V = 1243.6 (7) Å^3, Z = 2, d_{calcd} = 1.655 g/cm^3. Full-matrix refinement (based on F_o^2) with anisotropic temperature factors for the 32 non-hydrogen and isotropic temperature factors for the 26 hydrogen atoms converged with discrepancy indices of $R(F_o)$ = 0.043, $R(F_o^2)$ = 0.045 and $R_w(F_o^2)$ = 0.075 with σ_1 = 1.57 for 2914 data with $F_o^2 > \sigma(F_o^2)$. A table of refined positional and thermal parameters is included with the supplementary material.

(32) Reddy, K. P.; Petersen, J. L. *Organometallics* **1989**, *8*, 547.

Distinction among Three Possible Radical Chain Mechanisms in the Disproportionation Reactions of $Cp_2Fe_2(CO)_4$ ($Cp = \eta^5\text{-}C_5H_5$)

Michael P. Castellani and David R. Tyler*

Department of Chemistry, University of Oregon, Eugene, Oregon 97403

Received December 22, 1988

The kinetics of the thermal disproportionation reaction of the $Cp_2Fe_2(CO)_4$ complex with dppe (1,2-bis(diphenylphosphino)ethane) were studied so as to differentiate between three possible radical chain mechanisms. The disproportionation reaction is initiated by spontaneous homolysis of the Fe-Fe bond at room temperature in CH_2Cl_2 ($k \approx 2.7 \times 10^{-7}$ s^{-1}). The rate law for the disproportionation reaction is rate = k[dppe]$^{1/2}$[$Cp_2Fe_2(CO)_4$], where $k = 7.0 \times 10^{-4}$ M$^{-1/2}$ s^{-1} at 23 °C in CH_2Cl_2. This rate law is consistent with the radical chain pathway in Scheme I (in which ligand association to a 17-electron $CpFe(CO)_2$ radical is followed by electron transfer and then a fragmentation step) but not with the pathways in Schemes II and III (which involve variations in the sequence of the association, electron transfer, and fragmentation steps). The thermal disproportionation reaction of $Cp_2Fe_2(CO)_4$ with dppe is inhibited by trace impurities in the reaction solution; the reaction could be initiated, however, by brief irradiation of the reaction solution. Presumably, the impurities are removed by reaction with the intermediates formed in the photoreaction. Analysis of the kinetics data by the numerical integration program GIT yielded values for the unknown rate constants in the disproportionation mechanism, including the values for the equilibrium constant for the reaction of $CpFe(CO)_2$ with dppe to form the 19-electron $CpFe(CO)_2$(dppe-P) complex (K_{eq} = 0.91) and for the termination step in which $CpFe(CO)_2$ reacts with CpFe(CO)dppe ($k = 7.8 \times 10^7$ M^{-1} s^{-1}). The kinetic chain length for the reaction was calculated to be 460.

Introduction

In a series of papers, we reported the results of our mechanistic studies of the photochemical disproportionation reactions of the $Cp_2Fe_2(CO)_4$,[1] $Cp_2Mo_2(CO)_6$,[2] and $Mn_2(CO)_{10}$[3] complexes (eq 1, shown for the case of

$$Cp_2Fe_2(CO)_4 + L \xrightarrow{h\nu} CpFe(CO)_2L^+ + CpFe(CO)_2^- \quad (1)$$

$$L = PR_3, P(OR)_3$$

$Cp_2Fe_2(CO)_4$;[4] analogous reactions occur with the other dimers). The reactions follow a chain pathway, and the

0276-7333/89/2308-2113$01.50/0

Scheme I

$$Cp_2Fe_2(CO)_4 \overset{h\nu}{\rightleftharpoons} \underset{17e}{2CpFe(CO)_2} \quad \text{initiation} \quad (2)$$

$$\underset{17e}{CpFe(CO)_2} + L \overset{K_{eq}}{\rightleftharpoons} \underset{19e}{CpFe(CO)_2L} \quad \text{ligand association} \quad (3)$$

$$\underset{19e}{CpFe(CO)_2L} + Cp_2Fe_2(CO)_4 \longrightarrow CpFe(CO)_2L^+ + Cp_2Fe_2(CO)_4^- \quad \text{electron transfer} \quad (4)$$

$$Cp_2Fe_2(CO)_4^- \longrightarrow CpFe(CO)_2^- + \underset{17e}{CpFe(CO)_2} \quad \text{fragmentation} \quad (5)$$

$$\underset{19e}{CpFe(CO)_2L} + \underset{17e}{CpFe(CO)_2} \longrightarrow CpFe(CO)_2L^+ + CpFe(CO)_2^- \quad \text{termination} \quad (6)$$

mechanism in Scheme I was proposed.[1] Analogous pathways were also proposed to operate with the other dimer complexes.[2,3]

The steps in the chain pathway are (1) ligand association (eq 3), (2) electron transfer (eq 4), and (3) fragmentation (eq 5). Considerable experimental evidence and literature precedents exist for each of these steps. For example, we demonstrated that the electron transfer in eq 4 is a reasonable reaction because the 19-electron adducts are powerful reductants.[1,5] Likewise, pulse radiolysis studies established that fragmentation (eq 5) occurs when the $M_2(CO)_{10}$ (M = Mn, Re) dimers are reduced;[6] by analogy, it seemed reasonable to suggest that similar fragmentations also occurred when the other metal–metal bonded dimers were reduced. Furthermore, electrochemical reductions of metal carbonyl dimers are generally irreversible (to give two ML_n^- molecules), a behavior attributed to the fast fragmentation of the reduced dimer as shown in eq 5.[7]

Despite the evidence and precedents for each of the individual steps in the chain process (ligand association, electron transfer, and fragmentation), other chain mechanisms, involving different sequences of the basic steps, are possible. For example, fragmentation of the reduced dimer (e.g. $Cp_2Fe_2(CO)_4^-$) might not be so fast as to exclude the mechanism in Scheme II. In this pathway, fragmentation of the reduced dimer is not spontaneous but is induced by reaction with the ligand (eq 10). This possibility is particularly attractive for the case of the $Cp_2Fe_2(CO)_4$ dimer because this molecule has bridging carbonyl ligands which might prevent fragmentation of the reduced dimer.[8]

Scheme II

$$Cp_2Fe_2(CO)_4 \overset{h\nu}{\rightleftharpoons} \underset{17e}{2CpFe(CO)_2} \quad (7)$$

$$\underset{17e}{CpFe(CO)_2} + L \rightleftharpoons \underset{19e}{CpFe(CO)_2L} \quad \text{initiation} \quad (8)$$

$$\underset{19e}{CpFe(CO)_2L} + Cp_2Fe_2(CO)_4 \longrightarrow CpFe(CO)_2L^+ + Cp_2Fe_2(CO)_4^- \quad \text{electron transfer} \quad (9)$$

$$Cp_2Fe_2(CO)_4^- + L \longrightarrow Cp_2Fe_2(CO)_4L^- \quad \text{ligand association}^8 \quad (10)$$

$$Cp_2Fe_2(CO)_4L^- \longrightarrow CpFe(CO)_2^- + \underset{19e}{CpFe(CO)_2L} \quad \text{fragmentation}^8 \quad (11)$$

Scheme III

$$Cp_2Fe_2(CO)_4 \overset{h\nu}{\rightleftharpoons} \underset{17e}{2CpFe(CO)_2} \quad (12)$$

$$\underset{17e}{CpFe(CO)_2} + L \rightleftharpoons \underset{19e}{CpFe(CO)_2L} \quad \text{initiation} \quad (13)$$

$$\underset{19e}{CpFe(CO)_2L} + Cp_2Fe_2(CO)_4 \longrightarrow CpFe(CO)_2L^+ + Cp_2Fe_2(CO)_4^- \quad (14)$$

$$Cp_2Fe_2(CO)_4^- + L \rightleftharpoons Cp_2Fe_2(CO)_4L^- \quad \text{ligand association} \quad (15)$$

$$Cp_2Fe_2(CO)_4L^- + Cp_2Fe_2(CO)_4 \longrightarrow Cp_2Fe_2(CO)_4L + Cp_2Fe_2(CO)_4^- \quad \text{electron transfer} \quad (16)$$

$$Cp_2Fe_2(CO)_4L \longrightarrow CpFe(CO)_2L^+ + CpFe(CO)_2^- \quad \text{fragmentation} \quad (17)$$

Note that the sequence of steps in this chain is electron transfer, followed by ligand association and then fragmentation. Likewise, Scheme III shows a pathway that could result if reaction of the reduced dimer with the ligand did not lead to fragmentation.[9] Instead, the $Cp_2Fe_2(CO)_4L^-$ adduct transfers an electron to an unreacted dimer molecule. In this scheme, the sequence of reactions is ligand association followed by electron transfer, and the fragmentation is not part of the chain.[10]

In order to complete our investigation of the mechanism of the disproportionation reactions of the metal–metal bonded carbonyl dimers, it was necessary to differentiate between the chain pathways outlined in Schemes I–III. As we explain in the Discussion, such differentiation is not possible with photochemical kinetics methods but is possible with thermal kinetics. In this paper, we report the results of our study of the thermal disproportionation reaction of the $Cp_2Fe_2(CO)_4$ complex with dppe. The results allowed us to eliminate two of the pathways in Schemes I–III. Perhaps of most importance, our results delineate several new fundamental principles that will contribute to the general knowledge of quantitative organometallic radical chemistry.

(1) Goldman, A. S.; Tyler, D. R. *Inorg. Chem.* **1987**, *26*, 253–258.

(2) (a) Stiegman, A. E.; Stieglitz, M.; Tyler, D. R. *J. Am. Chem. Soc.* **1983**, *105*, 6032–6037. (b) Stiegman, A. E.; Tyler, D. R. *J. Am. Chem. Soc.* **1982**, *104*, 2944–2945. (c) Philbin, C. E.; Goldman, A. S.; Tyler, D. R. *Inorg. Chem.* **1986**, *25*, 4434–4436. (d) Goldman, A. S.; Tyler, D. R. *J. Am. Chem. Soc.* **1984**, *106*, 4066–4067. (e) Philbin, C. E.; Granatir, C. A.; Tyler, D. R. *Inorg. Chem.* **1986**, *25*, 4806. (f) Stiegman, A. E.; Tyler, D. R. *J. Am. Chem. Soc.* **1985**, *107*, 967–971.

(3) (a) Stiegman, A. E.; Tyler, D. R. *Inorg. Chem.* **1984**, *23*, 527–529. (b) Stiegman, A. E.; Goldman, A. S.; Philbin, C. E.; Tyler, D. R. *Inorg. Chem.* **1986**, *25*, 2976–2979.

(4) With many monodentate ligands, $CpFe(CO)L_2^+$ is also formed in the reaction. With bidentate ligands, the only cationic product is $CpFe(CO)(L_2)^+$.

(5) (a) Stiegman, A. E.; Goldman, A. S.; Leslie, D. B.; Tyler, D. R. *J. Chem. Soc., Chem. Commun.* **1984**, 632–633. (b) MacKenzie, V.; Tyler, D. R. *J. Chem. Soc., Chem. Commun.* **1987**, 1783–1784.

(6) (a) Waltz, W. L.; Hackelberg, O.; Dorfman, L. M.; Wojcicki, A. *J. Am. Chem. Soc.* **1978**, *100*, 7259–7263. (b) Meckstroth, W. K.; Walters, R. T.; Waltz, W. L.; Wojcicki, A.; Dorfman, L. M. *J. Am. Chem. Soc.* **1982**, *104*, 1842–1846.

(7) Dessy, R. E.; Weissman, P. M.; Pohl, R. L. *J. Am. Chem. Soc.* **1966**, *88*, 5117–5121.

(8) The reaction of $Cp_2Fe_2(CO)_4^-$ with L in Scheme II is shown to produce $Cp_2Fe_2(CO)_4L^-$. This latter species may not actually be an intermediate because the reaction with L may induce fragmentation directly so that the reaction is a combination of the ligand association and fragmentation steps without the intermediate formation of $Cp_2Fe_2(CO)_4L^-$, i.e. $Cp_2Fe_2(CO)_4^- + L \rightarrow CpFe(CO)_2^- + CpFe(CO)_2L$.

(9) There are several precedents for proposing the step (eq 15) in which a ligand forms an adduct with a dimer molecule (although not a reduced dimer, as shown in Scheme III). See: (a) Tyler, D. R.; Schmidt, M. A.; Gray, H. B. *J. Am. Chem. Soc.* **1979**, *101*, 2753–2755. (b) Tyler, D. R.; Schmidt, M. A.; Gray, H. B. *J. Am. Chem. Soc.* **1983**, *105*, 6018–6021. (c) Absi-Halabi, M.; Atwood, J. D.; Forbus, N. P.; Brown, T. L. *J. Am. Chem. Soc.* **1980**, *102*, 6248–6254. (d) Forbus, N. P.; Oteiza, R.; Smith, S. G.; Brown, T. L. *J. Organomet. Chem.* **1980**, *193*, C71–C74. (e) Starghelli, P. L.; Rosetti, R.; Mentasti, E.; Pelizzetti, E. *Inorg. Chim. Acta* **1977**, *22*, 19–22.

(10) Note that all of the mechanisms in Schemes I–III are electron-transfer-chain (ETC) catalyzed pathways. For other reviews of ETC reactions, see: (a) Julliard, M.; Chanon, M. *Chem. Rev.* **1983**, *83*, 425–506. (b) Channon, M. *Bull. Soc. Chim. Fr.* **1982**, 197–240. (c) Saveant, J. M. *Acc. Chem. Res.* **1980**, *13*, 323–329. (d) Chanon, M.; Tobe, M. L. *Angew. Chem., Int. Ed. Engl.* **1982**, *21*, 1–86.

Experimental Section

All manipulations of air-sensitive materials were carried out under a nitrogen atmosphere by using standard Schlenk or vacuum line techniques. When appropriate, solids and solutions were handled under a nitrogen atmosphere in a Vacuum Atmospheres glovebox.

Materials. Dichloromethane was refluxed over CaH_2 and distilled under nitrogen. Pentane was refluxed over sodium and distilled under nitrogen. Carbon tetrachloride was refluxed over P_2O_5 and distilled under nitrogen. 1,2-Bis(diphenylphosphino)ethane, dppe (Strem), was purified by multiple recrystallizations from hot 95% aqueous ethanol. $Cp_2Fe_2(CO)_4$ was synthesized by the method of King[11] and recrystallized several times from CH_2Cl_2/pentane. $Ph_2P(O)CH_2CH_2(O)PPh_2$ was prepared by the method of Hoffmann et al.[12]

Instruments and Techniques. Photochemical reactions were carried out with an Oriel 200-W high-pressure mercury arc lamp. A 505-nm interference filter (Edmund Scientific) or a Corning CS 3-68 filter ($\lambda > 525$ nm) was used to isolate the desired wavelengths. Infrared and electronic absorption spectra were obtained with Nicolet 5DBX FT-IR and Beckman DU spectrophotometers, respectively. Proton NMR spectra were obtained on a GE QE-300 spectrometer at 300.15 MHz. EPR spectra were measured on a Varian E-9 spectrometer.

In a typical experiment, 7.8 mg of $Cp_2Fe_2(CO)_4$ (2.2×10^{-5} mol) and 0.20 g of dppe (5.0×10^{-4} mol) were placed in a 10-mL volumetric flask equipped with a 7-mm magnetic stir bar which was then transferred to the glovebox. In a minimum of light, CH_2Cl_2 was added to bring the volume to 10 mL and the flask was quickly wrapped in aluminum foil. After the solution was stirred for 5 min, 3 mL of solution was transferred rapidly to a Pyrex cell[13] that was then wrapped in a black cloth. The cell was moved to a dark room where the solution was degassed by four freeze–pump–thaw cycles on a vacuum line in the dark. The solution was irradiated with stirring at 505 nm in 15–60-s increments until a rapid drop in the absorbance at 520 nm[14] was observed. The irradiation was stopped, and thereafter absorbance measurements were taken at fixed time intervals that depended on the dppe concentration. Brief exposure to the dim red light used in the dark room had no effect on the solutions either before or after irradiation.

Dark Reaction of $Cp_2Fe_2(CO)_4$ with CCl_4. $Cp_2Fe_2(CO)_4$ (2.6 mg, 7.3×10^{-6} mol) was placed in the side arm, and 3 mL of CCl_4 was placed in the bulb of a cell described earlier.[13] In the dark, the $Cp_2Fe_2(CO)_4$ was dissolved by shaking the cell. A dim red light was briefly turned on (for several seconds) to confirm that the solid was completely dissolved. Thereafter the cell was handled and stored rigorously in the dark. An infrared spectrum of the solution (after 30 days) showed that significant reaction had taken place. The infrared solution cell was loaded in a minimum of light, and a silicon wafer was taped to the cell window to filter out visible or UV light from the source that might cause a photochemical reaction to take place.

Method of Kinetics Analysis. The A_∞ values for each run were obtained by the Kezdy–Swinborne[15] method. A plot of ln $[(A - A_\infty)/(A_0 - A_\infty)]$ vs time was then used to calculate the k_{obs} for each run.

Results

The Rate Laws. The rate laws for the three radical chain pathways in Schemes I–III depend on the relative ratios of the rate constants. The rate expressions below are those for the most likely relative rates. Complete derivations of these and the other expressions are provided in the Appendix. The rate expressions are shown for the case L = dppe.

Table I. Relevant Infrared Spectroscopic Data in CH_2Cl_2[a]

complex	IR ν(CO), cm^{-1}
$Cp_2Fe_2(CO)_4$	1988 s, 1956 ms, 1769 s
[CpFe(CO)dppe]Cl	1981
$CpFe(CO)_2(CH_2Cl)$	2023 m, 1966 s

[a] See ref 1.

For the pathway in Scheme I

$$\frac{-d[Cp_2Fe_2(CO)_4]}{dt} = k[dppe]^{1/2}[Cp_2Fe_2(CO)_4] \quad (18)$$

For the pathway in Scheme II

$$\frac{-d[Cp_2Fe_2(CO)_4]}{dt} = k[dppe][Cp_2Fe_2(CO)_4] \quad (19)$$

For the pathway in Scheme III

$$\frac{-d[Cp_2Fe_2(CO)_4]}{dt} = k[dppe]^2[Cp_2Fe_2(CO)_4] \quad (20)$$

Note that the three rate expressions are different, and it should be possible, therefore, to differentiate between the three pathways.

Choice of Solvent. Our previous study showed that no net disproportionation of the $Cp_2Fe_2(CO)_4$ dimer occurred in most solvents (with a wide variety of monodentate and bidentate phosphines, including dppe) because of a facile back-reaction between $CpFe(CO)_2^-$ and $CpFe(CO)_2PR_3^+$.[1] However, CH_2Cl_2 completely prevented the back-reaction by reacting quickly with $CpFe(CO)_2^-$ according to eq 21; thus, CH_2Cl_2 was the solvent used in this study.

$$CpFe(CO)_2^- + CH_2Cl_2 \rightarrow CpFe(CO)_2(CH_2Cl) + Cl^- \quad (21)$$

Dark Reactions with dppe. Control experiments showed that CH_2Cl_2 solutions of $Cp_2Fe_2(CO)_4$ and dppe are stable for at least 12 h in the dark. However, after brief irradiation of the solution ($\lambda = 505$ nm), a reaction began and continued in the dark until all of the $Cp_2Fe_2(CO)_4$ was consumed[16] or until an inhibitor was added.[17] (See below for a further discussion of the induction period.) Infrared analysis of the reaction solution (Table I) showed that $CpFe(CO)_2(CH_2Cl)$ and $CpFe(CO)dppe^+$ formed quantitatively in the dark reaction. Thus, the thermal disproportionation reaction with dppe is the same as the photochemical reaction reported previously:[1]

$$Cp_2Fe_2(CO)_4 + dppe + CH_2Cl_2 \rightarrow CpFe(CO)dppe^+ + CpFe(CO)_2(CH_2Cl) + Cl^- + CO \quad (22)$$

The rate of the dark reaction is first-order in $Cp_2Fe_2(CO)_4$ and half-order in dppe. Figure 1 is a plot of ln $[(A - A_\infty)/(A_0 - A_\infty)]$ vs time for several reactions run under

(11) King, R. B. *Organometallic Synthesis*; Academic: New York, 1965; Vol. 1, pp 114–116.
(12) Hoffmann, H.; Gruenewald, R.; Horner, L. *Chem. Ber.* **1960**, *93*, 861–865.
(13) The cell was connected by a side arm to an adjoining bulb used for degassing. The solution was then moved to the cell by tilting the apparatus. The cell was equipped with a Teflon screw-in plug to seal against the atmosphere.
(14) The lowest energy peak in the electronic spectrum of $Cp_2Fe_2(CO)_4$ is at 520 nm.
(15) Moore, J. W.; Pearson, R. G. *Kinetics and Mechanism*, 3rd ed.; Wiley-Interscience: New York, 1981; p 72.
(16) With very low concentrations of dppe, the time required for all of the $Cp_2Fe_2(CO)_4$ to react in the dark reaction was over 12 h. Note that the quantum yield of the photochemical disproportionation reaction is $\approx 10^2$.[1] Thus, with typical light intensities (say 2×10^{-7} einsteins min^{-1}), the dark reaction with dppe is considerably slower (rate $\leq 1 \times 10^{-7}$ M s^{-1}) than the photochemical reaction (rate $\approx 1 \times 10^{-4}$ M s^{-1}).
(17) The dark reaction can be inhibited with reducible substrates. For example, when *n*-butylpyridinium chloride (<0.1 mg) was added to a solution (3 mL) of $Cp_2Fe_2(CO)_4$ (2.2 mM) and dppe (0.1 mM) that had been irradiated and was reacting thermally, the reaction stopped. Our explanation is that the 19-electron CpFe(CO)dppe complex can reduce *n*-butylpyridinium,[1,5a] thereby removing CpFe(CO)dppe from the chain cycle.

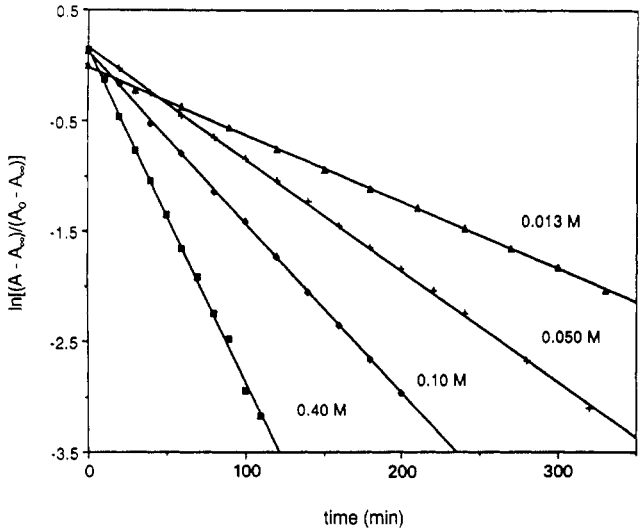

Figure 1. Plots of ln $[(A - A_\infty)/(A_0 - A_\infty)]$ vs time for the disproportionation reaction of $Cp_2Fe_2(CO)_4$ (2.2 mM) with dppe (13, 50, 100, 400 mM) at 23 °C in CH_2Cl_2. The disappearance of $Cp_2Fe_2(CO)_4$ was monitored at 520 nm.

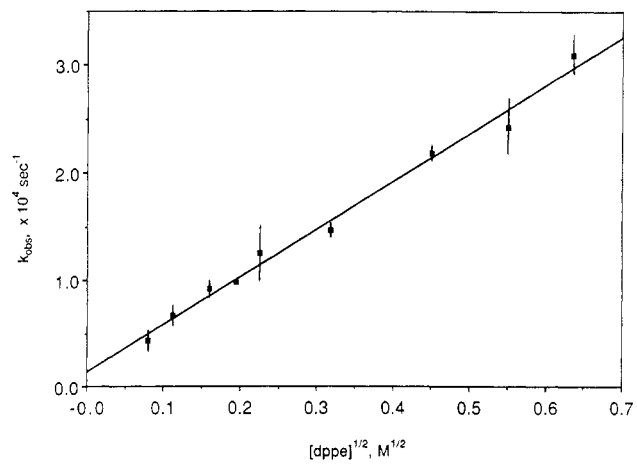

Figure 2. Plot of k_{obs} vs $[dppe]^{1/2}$ for the disproportionation reaction of $Cp_2Fe_2(CO)_4$ (2.2 mM) with dppe at 23 °C in CH_2Cl_2. The errors shown are one standard deviation.

pseudo first-order conditions at different concentrations of dppe. From these and other similar experiments, the plot in Figure 2 was constructed, showing the half-order dependence of the rate on the concentration of dppe. The overall rate expression is thus rate = $k[dppe]^{1/2}[Cp_2Fe_2(CO)_4]$, with $k = 7.0 \times 10^{-4}$ $M^{-1/2}$ s^{-1} at 23 °C.

The Induction Period. Irradiation of the solution containing $Cp_2Fe_2(CO)_4$ and dppe was necessary before the dark reaction began. Less than 3% of the $Cp_2Fe_2(CO)_4$ was typically consumed during the irradiation period. Three factors influenced the length of the photochemical induction period. First, the induction period increased with increasing concentration of dppe. The induction times for a given concentration of dppe varied, but typical data are given in Table II. These data suggest that an inhibitor is present as an impurity in the dppe; however, multiple recrystallizations of the dppe did not shorten the induction times. A logical impurity in the dppe that might have been acting as the inhibitor is dppe oxide, $Ph_2P(O)CH_2CH_2P(O)Ph_2$. Addition of this compound (0.23 mM, about 10 mol % of $Cp_2Fe_2(CO)_4$) to the reaction solutions, however, did not change the induction times. Ethanol, the solvent used to recrystallize the dppe, was another suspected impurity. However, deliberate addition of 95% ethanol (1.1×10^{-5} M, 0.5 mol % $Cp_2Fe_2(CO)_4$) to the reaction solutions also did not alter the induction time.

Table II. Irradiation[a] Times Required To Start the Dark Reactions[b,c]

[dppe], M	irradiatn time, min	[dppe], M	irradiatn time, min
1.25×10^{-2}	3, 5	1.0×10^{-1}	3, 3
2.5×10^{-2}	1.5, 1	2.0×10^{-1}	4, 4
3.8×10^{-2}	1.5, 1	4.0×10^{-1}	14, 9
5.0×10^{-2}	3, 2, 2		

[a] $\lambda = 505$ nm; $I_a \approx 3 \times 10^{-8}$ einstein L^{-1} min^{-1}. [b] $[Cp_2Fe_2(CO)_4] \approx 2.2$ mM. [c] The reaction solutions were monitored at 15-s intervals to check for the start of the dark reaction.

The induction period is also dependent on the intensity of the absorbed radiation. Thus, when the radiation intensity was 1×10^{-10} einstein min^{-1}, the induction period was typically 1–10 min (depending on the dppe concentration); at 8×10^{-9} einstein min^{-1}, the induction period was only several seconds for comparable reaction conditions.

Finally, the induction times increased about 30% when the reaction solutions were not rigorously degassed by any freeze–pump–thaw cycles. (The solutions were still prepared in the glovebox (see Experimental Section), so they are nominally oxygen-free: $[O_2] \leq 3$ ppm.) This result suggests that oxygen may also play a minor role in the inhibition of the dark reaction.

Control experiments showed that the rate of the dark reaction was independent of the irradiation time used to start the reaction. Thus, irradiation of the reaction solutions beyond the minimum time required to initiate the dark reaction (with concomitant consumption of $Cp_2Fe_2(CO)_4$ in the photochemical disproportionation reaction[1,16]) did not change the rate of the dark reaction relative to the rate for a similar solution irradiated for the minimum time required to initiate the dark reaction.

ESR Results. A CH_2Cl_2 solution of $Cp_2Fe_2(CO)_4$ (2.2 mM) and dppe (0.1 mM) was prepared under nitrogen in an ESR tube and irradiated ($\lambda > 525$ nm) in order to start the dark reaction. The solution was ESR silent throughout the course of the dark reaction.

Reaction with CCl_4. The dark reaction of $Cp_2Fe_2(CO)_4$ with CCl_4 was carried out under rigorously dark conditions (see the Experimental Section for details). A 2.4 mM solution of $Cp_2Fe_2(CO)_4$ in CCl_4 was prepared and set aside in the dark. After 30 days, an infrared spectrum of the solution showed the disappearance of about half the $Cp_2Fe_2(CO)_4$ and the appearance of $CpFe(CO)_2Cl$. No other species were observed, and we conclude that reaction 23 need not be photochemically initiated.

$$Cp_2Fe_2(CO)_4 \xrightarrow[CCl_4]{\text{dark, room temp}} 2CpFe(CO)_2Cl \quad (23)$$

Discussion

The Thermal Reaction of $Cp_2Fe_2(CO)_4$ with dppe. We decided not to try and differentiate between the mechanisms in Schemes I–III by studying the kinetics of reactions initiated by metal–metal bond photolysis because there is considerable scatter in the disproportionation reaction quantum yields. Because of the scatter, it would not be possible to measure the quantum yields with the precision required to distinguish between the photochemical rate laws for the three pathways. However, as the rate expressions in eq 18–20 show, if the metal–metal bond homolysis occurred thermally, then the rate expressions for the three pathways would be different, and it should be possible to differentiate between the pathways. The

$Cp_2Fe_2(CO)_4$ dimer was selected for study because in our previous investigation of this complex, we showed that spontaneous homolysis of the Fe–Fe bond occurred at a slow rate at room temperature in solution.[18]

Dppe was chosen as the ligand in this study because our previous study[1] also showed that disproportionation, but no substitution, occurred in the photochemical reaction of $Cp_2Fe_2(CO)_4$ with this ligand in CH_2Cl_2 solution. Infrared analysis showed that the thermal reaction of $Cp_2Fe_2(CO)_4$ with dppe also resulted only in disproportionation, and therefore the kinetics studies were not complicated by a substitution side reaction.

Another advantage of a thermal study is that there are no complications arising from a CO-loss pathway. Numerous workers have demonstrated that both M–M homolysis and M–CO dissociation generally result from low-energy irradiation of metal–metal bonded dimers.[19] However, our results showed that no reaction occurred when $Cp_2Fe_2(CO)_4$ and phosphines or phosphites were mixed in CH_2Cl_2 and kept in the dark at room temperature. Were Fe–CO bond dissociation occurring, then some substitution of the $Cp_2Fe_2(CO)_4$ would undoubtedly have resulted. We conclude therefore that Fe–CO bond dissociation does not occur at room temperature and that the kinetics studies will not be complicated by side reactions resulting from a process other than Fe–Fe bond homolysis.

The Radical Chain Mechanism. The rate law for the thermal disproportionation of $Cp_2Fe_2(CO)_4$ with dppe was found to be that in eq 18. This result would seem to imply that the mechanism in Scheme I is followed, but other pathways could conceivably give the same rate law. However, as we discuss next, various results clearly establish that the thermal disproportionation reactions with dppe follow a radical chain pathway, specifically the one in Scheme I. Evidence for a radical mechanism comes from the overall $^3/_2$-order in the rate expression. Rate laws of $^3/_2$-order are common for radical mechanisms,[20] but it is impossible to write a chemically reasonable non-radical mechanism that has this rate law. Evidence for the chain nature of the reaction comes from a comparison of the disproportionation reaction rates with the rate for the reaction with CCl_4. The reaction with CCl_4 to give $CpFe(CO)_2Cl$ (eq 23) follows the pathway shown in Scheme IV.[21] High concentrations of carbon tetrachloride quantitatively trap $CpFe(CO)_2$ free radicals, and thus the rate of reaction 23 is equal to the rate of $CpFe(CO)_2$ free radical production. The disproportionation reactions are complete in a matter of minutes to hours ($k = 7.0 \times 10^{-4}$ $M^{-1/2}$ s^{-1}), yet the reaction of a comparable concentration of $Cp_2Fe_2(CO)_4$ with CCl_4 (eq 23) is only approximately half complete after 30 days ($k \approx 2.7 \times 10^{-7}$ s^{-1}). Only a chain reaction or a bimolecular reaction of $Cp_2Fe_2(CO)_4$ with dppe can account for the increase in the disproportionation rates relative to the rate of thermal homolysis. The rate law rules out the bimolecular reaction possibility, however, and a chain mechanism is implied. This result, combined with the evidence for a radical mechanism, establishes that the thermal reaction follows a radical chain mechanism. The specific form of the rate law establishes that the radical chain pathway is that shown in Scheme I.

Scheme IV

$$Cp_2Fe_2(CO)_4 \rightleftharpoons 2CpFe(CO)_2$$

$$CpFe(CO)_2 + CCl_4 \rightarrow CpFe(CO)_2Cl + CCl_3$$

Establishing that the thermal disproportionation reaction follows a radical chain mechanism is an important result because it shows that the mechanisms of the thermal and the photochemical reactions are identical. Although this conclusion would seem to follow logically because the $CpFe(CO)_2$ intermediate is formed in the photochemical reactions and it forms in the thermal reactions, it was by no means certain that the slow rate of thermal homolysis (and the subsequent chain reaction) would contribute to any significant extent to the thermal disproportionation reaction; i.e., a faster bimolecular pathway involving reaction of $Cp_2Fe_2(CO)_4$ with dppe was possible. However, because the thermal and photochemical reactions both follow chain pathways and because the $CpFe(CO)_2$ intermediate is common to both systems, we conclude that the chain portions of the thermal and photochemical reactions are identical. The important conclusion is that because the thermal and photochemical pathways are the same (except for the mechanism of initiation), mechanistic conclusions drawn from the thermal kinetics studies apply to the photochemical reaction as well. Thus, the mechanism of the photochemical disproportionation reactions is also that shown in Scheme I. This pathway is the one proposed in our previous photochemical papers.[1-3]

Inhibition. As pointed out in the Results, the major factor that determines the length of the induction period is the concentration of dppe. Our results showed that neither dppe oxide, ethanol (the recrystallization solvent), nor water were inhibitors, and we suggest therefore that some other impurity in the dppe inhibits the chain reaction. The impurities are apparently removed during the photolysis process, presumably by reaction with chain-carrying intermediates. The effect of oxygen on the induction period can be explained similarly. Oxygen can combine with the $CpFe(CO)_2$ radical,[6a] or it could oxidize the 19-electron CpFe(CO)dppe species[4] and thereby prevent these chain-carrying molecules from participating in the chain.

Analysis of the Rate Constants. The kinetics data from the experiments with dppe concentrations of 2.5×10^{-2}, 2.0×10^{-1}, and 3.0×10^{-1} M were analyzed by the numerical integration program GIT.[22] The data were fit to the pathway in Scheme V, and the rate constants k_3, k_4, k_5, k_6, k_7, and k_8 were allowed to vary. (The dppe-P nomenclature indicates only one P atom in the dppe ligand is bonded to the Fe atom.) (Scheme V is Scheme I with

(18) The set of experiments that showed this was the following.[1] A control solution of $(MeCp)_2Fe_2(CO)_4$ (15 mM) and $Cp_2Fe_2(CO)_4$ (15 mM) in acetone-d_6 was found to be stable for 24 h at room temperature in the dark, showing only very slight "scrambling" (cross coupling): $(MeCp)_2Fe_2(CO)_4 + Cp_2Fe_2(CO)_4 \rightleftharpoons 2(MeCp)(Cp)Fe_2(CO)_4$. (As expected, irradiation of this solution induced the cross-coupling reaction, as determined by monitoring the ^1H NMR C_5H_5 resonance ($\delta_{Cp,Cp_2Fe_2(CO)_4} = 4.945$, $\delta_{Cp,(MeCp)(Cp)Fe_2(CO)_4} = 4.922$.) However, addition in the dark of dppe (30 mM) to an unscrambled solution resulted in a quick (<5 min) scrambling reaction; i.e., a 2:1 ratio of $(MeCp)(Cp)Fe_2(CO)_4$ to $Cp_2Fe_2(CO)_4$ was obtained. Our interpretation of these results was that the rate of Fe–Fe homolysis at room temperature is so small that negligible scrambling occurs via the direct cross-coupling of $(MeCp)Fe(CO)_2$ and $CpFe(CO)_2$ radicals. However, when dppe is added, the slight rate of homolysis is sufficient to initiate the disproportionation chain reaction. This leads to scrambling because, as we also showed, the disproportionation products back-react quickly in most solvents.[1] (Recall that the occurrence of a back-reaction in most solvents is one of the reasons why CH_2Cl_2 was used as the solvent in this study; the $CpFe(CO)_2^-$ anion reacts with CH_2Cl_2 to yield $CpFe(CO)_2(CH_2Cl)$ and the back-reaction is prevented.)

(19) Meyer, T. J.; Caspar, J. V. *Chem. Rev.* **1985**, *85*, 187–218.

(20) Huyser, E. S. *Free Radical Chain Reactions*; Wiley-Interscience: New York, 1970.

(21) Abrahamson, H. B.; Palazzotto, M. C.; Reichel, C. L.; Wrighton, M. S. *J. Am. Chem. Soc.* **1979**, *101*, 4123–4127.

(22) (a) Stabler, R. N.; Chesick, J. *Int. J. Chem. Kinet.* **1978**, *10*, 461–469. (b) McKinney, R. J.; Weigert, F. J. Quantum Chemistry Program Exchange, Program No. QCMP022. (c) Weigert, F. J. *Comput. Chem.* **1987**, *11*, 273.

Scheme V

$$Cp_2Fe_2(CO)_4 \underset{k_2}{\overset{k_1}{\rightleftharpoons}} 2CpFe(CO)_2 \quad (24)$$

$$CpFe(CO)_2 + dppe \underset{k_4}{\overset{k_3}{\rightleftharpoons}} CpFe(CO)_2(dppe\text{-}P) \quad (25)$$

$$CpFe(CO)_2(dppe\text{-}P) \underset{k_6}{\overset{k_5}{\rightleftharpoons}} CpFe(CO)(dppe) + CO \quad (26)$$

$$CpFe(CO)(dppe) + Cp_2Fe_2(CO)_4 \xrightarrow{k_7} CpFe(CO)(dppe)^+ + CpFe(CO)_2^- + CpFe(CO)_2 \quad (27)$$

$$CpFe(CO)dppe + CpFe(CO)_2 \xrightarrow{k_8} CpFe(CO)dppe^+ + CpFe(CO)_2^- \quad (28)$$

an additional step showing the stepwise coordination of the bidentate dppe ligand.) The rate constant k_2 was given the value 1×10^9, based on a reported measurement.[19] The value for k_1 (2.7×10^{-7} s^{-1}) was obtained in this study by the reaction of $Cp_2Fe_2(CO)_4$ with CCl_4. A good fit for all three sets of data was obtained for the following calculated values of the rate constants: $k_3 = 3.2 \times 10^7$ M^{-1} s^{-1}, $k_4 = 3.5 \times 10^7$ s^{-1}, $k_5 = 3.5 \times 10^5$ s^{-1}, $k_6 = 3.3 \times 10^{-3}$ M^{-1} s^{-1}, $k_7 = 5.0 \times 10^2$ M^{-1} s^{-1}, and $k_8 = 7.8 \times 10^7$ M^{-1} s^{-1}. (See ref 23 for an important discussion of error in these values. A plot showing the calculated curve and experimental data for the experiment with [dppe] = 2.5×10^{-2} M is shown in Figure 3.) In the Appendix, we show that k in eq 18 is equal to $(k_1k_3k_5k_7/k_4k_8)^{1/2}$. Substituting the calculated rate constants into this expression yields $k = 6.1 \times 10^{-4}$ M$^{-1/2}$ s^{-1}. This calculated value for k compares favorably with the experimental value of 7.0×10^{-4} M$^{-1/2}$ s^{-1} and can be taken as a "goodness of fit" indicator.

The numerical integration program can also be used to calculate the kinetic chain length of the reaction. The kinetic chain length is defined as the rate of the propagating reactions (they all have the same rate) divided by the sum of the rates of the termination reactions.[20] In order to determine this number for Scheme V, it was necessary to know the steady-state concentrations of the intermediates. These concentrations are difficult to determine experimentally, so they were calculated by using the program and the rate constants above. Thus, when [dppe] = 2.5×10^{-2} M and [$Cp_2Fe_2(CO)_4$] = 1.9×10^{-3} M, the following steady-state concentrations were calculated:

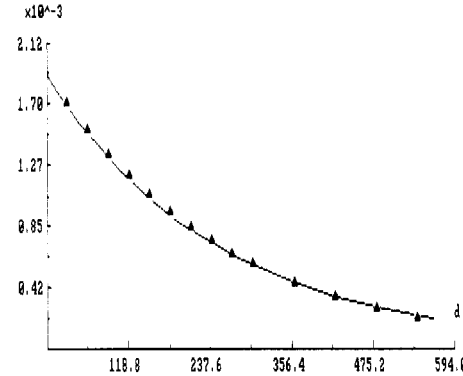

Figure 3. Plot of [$Cp_2Fe_2(CO)_4$] vs time for the reaction of $Cp_2Fe_2(CO)_4$ with dppe (2.5×10^{-2} M) in CH_2Cl_2 at 23 °C. The curve was generated by the numerical integrator GIT using the rate constants reported in the text. The experimental data are shown as triangles.

[$CpFe(CO)_2$] = 2.7×10^{-11} M, [$CpFe(CO)_2$(dppe-P)] = 6.0×10^{-13}, and [CpFe(CO)dppe] = 2.3×10^{-7} M. From these values, the kinetic chain length was calculated to be 4.6×10^2. It is interesting to note that the rate expressions for radical chain mechanisms are considerably easier to derive when it can be assumed that the chain length is relatively large.[20] In fact, this assumption was made in the Appendix for the derivation of rate equation 18 for Scheme V. The chain length of 460 justivies this assumption.

Generalizations. Several generalities concerning the reactivity and stability of organometallic radicals emerge from this study. For example, the calculated values of the rate constants demonstrate several interesting points. First, note that eq 25, the reaction of a 17-electron species with a ligand to form a 19-electron complex, is an equilibrium, and the equilibrium constant is about 0.91. This result is consistent with our[2e] and others[24] previous results which showed that the equilibrium constants for the formation of 19-electron species are generally in the range 1–1000. Note, however, that the reaction to form the chelated 19-electron complex (eq 26) is not reversible, and it is for this reason that chelating ligands are used to drive the formation of 19-electron complexes.[1] Also of interest is the value found for k_8, the rate constant for the termination step in eq 28. In previous experimental measurements of the equilibrium constants for the reactions of 17-electron complexes with ligands to form 19-electron complexes,[2e] we had to assume that this termination reaction was diffusion-controlled. The numerical integration analysis suggests, however, that such reactions may not be diffusion-controlled, and as a consequence, the equilibrium constants we calculated previously are too small. Thus, in these cases the 19-electron complexes are even more thermodynamically stable than we previously thought.[2e] Complete details of the numerical integration analysis of this and other related reactions as they relate to the determination of the equilibrium constants will be reported in a subsequent paper.[25] Finally, recall that in the Introduction, we suggested that the pathways in Schemes II and III might be reasonable because the $Cp_2Fe_2(CO)_4^-$ complex might not dissociate readily because

(23) The nature of the algorithm used in the numerical integration program is such that it is not always possible to get a "goodness of fit" of the data and the calculated values. However, as the curves provided in the supplementary material show, the experimental data are reproduced well by the rate constants reported in the text. A question of a different nature is: Are these rate constants a unique solution to the data? Clearly, the answer is no. For example, the calculated curve fit is relatively insensitive to the value assigned to k_6 because there is essentially no back-reaction between CO and CpFe(CO)dppe. Thus, k_6 can decrease (to 0, essentially), and no change in the calculated data is observed. The value reported for k_6 (3.3×10^{-3}) is the maximum value for which no change in the calculated curve is observed; values higher than 3.3×10^{-3} lead to a poorer fit with the data. After extensive trial and error, we also determined that the k_3/k_4 ratio must be as reported (this makes sense because this step is an equilibrium), but the values for k_3 (and hence k_4) can vary up to a factor of about 1.5. Similarly, the reported ratio of k_7 to k_8 is necessary for a good fit (5.0×10^2 to 7.8×10^7), but the individual values can vary by perhaps up to 1 order of magnitude (e.g. 5.0×10^1 and 7.8×10^6 still give a reasonable fit). It is important to note that there is little change in the calculated steady-state concentration of the intermediates if the rate constants above are changed to other acceptable values. These concentrations will change, however, if rate constants are chosen that give a poorer fit with the experimental data.

(24) The equilibrium constant for the following reaction was found to be about 7.

$$\underset{17e}{CpFe(CO)(PPh_3)CH_3^+} + py \underset{}{\overset{K_{eq}}{\rightleftharpoons}} \underset{19e}{CpFe(CO)(PPh_3)(py)CH_3^+}$$

See: Trogler, W. C.; Therien, M. J. *J. Am. Chem. Soc.* **1987**, *109*, 5127–5133.

(25) Philbin, C. E.; Granatir, C.; Castellani, M. P.; Ritter, R.; Tyler, D. R., manuscript in preparation.

of the bridging carbonyls. The kinetics results show, however, that dissociation occurs much faster than ligand association to $Cp_2Fe_2(CO)_4^-$ (i.e. eq 5 in Scheme I is faster than eq 10 in Scheme II or eq 15 in Scheme III). This result is probably general for other metal–metal bonded dimers, and thus bimolecular reactions of reduced dimers should be considered unlikely.

Acknowledgment is made to the National Science Foundation for the support of this work. D.R.T. acknowledges the Alfred P. Sloan Foundation for a fellowship. R. J. McKinney and F. J. Weigert are acknowledged for a copy of GIT.

Appendix

Derivation of Eq 18. The complete mechanism for disproportionation of $Cp_2Fe_2(CO)_4$ with dppe is shown in Scheme V. Because $CpFe(CO)_2$, dppe, and $CpFe(CO)_2$(dppe-P) are in equilibrium, eq 25 and 26 are combined in the derivation below. The disproportionation scheme thus becomes

$$Cp_2Fe_2(CO)_4 \underset{k_2}{\overset{k_1}{\rightleftharpoons}} 2CpFe(CO)_2$$

$$CpFe(CO)_2 + dppe \underset{k_6}{\overset{k'}{\rightleftharpoons}} CpFe(CO)dppe + CO$$

$$CpFe(CO)dppe + Cp_2Fe_2(CO)_4 \xrightarrow{k_7} CpFe(CO)dppe^+ + CpFe(CO)_2^- + CpFe(CO)_2$$

$$CpFe(CO)_2 + CpFe(CO)dppe \xrightarrow{k_8} CpFe(CO)dppe^+ + CpFe(CO)_2^-$$

Note that $k' = k_5K_{eq}$ where $K_{eq} = k_3/k_4$ in Scheme V. The rate expression for this reaction pathway is given by

$$\text{rate} = \frac{-d[Cp_2Fe_2(CO)_4]}{dt} = k_1[Cp_2Fe_2(CO)_4] + k_7[CpFe(CO)dppe][Cp_2Fe_2(CO)_4] - k_2[CpFe(CO)_2]^2 \quad \text{(A1)}$$

Because the chain sequence is long, the propagation rate is much greater than the initiation and termination rates. Thus, only the second term in this rate equation is significant, and therefore

$$\text{rate} = k_7[CpFe(CO)dppe][Cp_2Fe_2(CO)_4] \quad \text{(A2)}$$

For convenience, the following abbreviations are used in the rate expression derivation which follows: $Fe_2 = Cp_2Fe_2(CO)_4$; $Fe = CpFe(CO)_2$; L = dppe; FeL = CpFe(CO)dppe.

Invoking the steady-state approximation, we can write

$$0 = \frac{d[FeL]}{dt} = k'[Fe][L] - k_6[FeL][CO] - k_7[FeL][Fe_2] - k_8[FeL][Fe] \quad \text{(A3)}$$

Therefore

$$[FeL] = \frac{k'[Fe][L]}{k_6[CO] + k_7[Fe_2] + k_8[Fe]} \quad \text{(A4)}$$

Because the chain sequence is long, we have that $k_7[Fe_2] \gg k_8[Fe]$ and $k_7[Fe_2] \gg k_6[CO]$. Therefore

$$[FeL] = \frac{k'[Fe][L]}{k_7[Fe_2]} \quad \text{(A5)}$$

When the chain sequence is long, the rate of termination equals the rate of initiation. Therefore

$$0 = k_1[Fe_2] - k_2[Fe]^2 - k_8[Fe][FeL] \quad \text{(A6)}$$

Substituting (A5) in (A6) gives

$$0 = k_1[Fe_2] - k_2[Fe]^2 - k_8[Fe]\left[\frac{k'[Fe][L]}{k_7[Fe_2]}\right] \quad \text{(A7)}$$

This expression is now solved for [Fe]. Letting $k_9 = k'k_8/k_7$, we get

$$[Fe] = \left[\frac{k_1[Fe_2]}{k_2 + k_9[L]/[Fe_2]}\right]^{1/2} \quad \text{(A8)}$$

The expressions for [Fe] and [FeL] are now inserted into the rate expression:

$$\text{rate} = \frac{-d[Fe_2]}{dt} = k_7[FeL][Fe_2] = k'[L]\left[\frac{k_1}{k_2[Fe_2] + k_9[L]}\right]^{1/2}[Fe_2] \quad \text{(A9)}$$

There are two limiting cases: $k_2[Fe_2] \gg k_9[L]$ or $k_2[Fe_2] \ll k_9[L]$. The former case leads to rate = $k_{10}[L][Fe_2]^{1/2}$ and the latter to rate = $k_{11}[L]^{1/2}[Fe_2]$, where $k_{10} = k'(k_1/k_2)^{1/2}$ and $k_{11} = k'(k_1/k_9)^{1/2}$. Our analysis of Scheme V by the numerical integrator GIT shows that $k_2[Fe_2] \ll k_9[L]$ and hence

$$\text{rate} = k_{11}[L]^{1/2}[Fe_2] \quad \text{(A10)}$$

where $k_{11} = k'k_1^{1/2}k_9^{-1/2} = (k_1k_3k_5k_7/k_4k_8)^{1/2}$.

Derivation of Eq 19. The pathway is shown below (L = dppe).

$$Fe_2 \underset{k_{-1}}{\overset{k_1}{\rightleftharpoons}} 2Fe$$

$$Fe + L \xrightarrow{k_2} Fe\text{–}L + CO$$

$$Fe\text{–}L + Fe_2 \xrightarrow{k_3} FeL^+ + Fe_2^-$$

$$Fe_2^- + L \xrightarrow{k_4} Fe^- + Fe\text{–}L$$

$$Fe + FeL \xrightarrow{k_7} Fe^- + FeL^+$$

(Note that eq 10 and 11 in Scheme II were combined above for simplicity.[8] All chain-propagating steps occur with the same rate so this does not affect the results below.) The rate expression is

$$\frac{-d[Fe_2]}{dt} = +k_1[Fe_2] - k_{-1}[Fe]^2 + k_3[FeL][Fe_2] \quad \text{(B1)}$$

Because the chain sequence is long, this expression simplifies to

$$\text{rate} = k_3[FeL][Fe_2] \quad \text{(B2)}$$

It is thus necessary to find [FeL]. The steady-state approximations yield the following equations:

$$\frac{d[Fe]}{dt} = 0 = 2k_1[Fe_2] - 2k_{-1}[Fe]^2 - k_2[Fe][L] - k_7[Fe][FeL] \quad \text{(B3)}$$

$$\frac{d[FeL]}{dt} = 0 = k_2[Fe][L] - k_3[FeL][Fe_2] + k_4[Fe_2^-][L] - k_7[Fe][FeL] \quad \text{(B4)}$$

$$\frac{d[Fe_2^-]}{dt} = 0 = k_3[FeL][Fe_2] - k_4[Fe_2^-][L] \quad \text{(B5)}$$

Addition of (B4) and (B5) yields

$$0 = k_2[Fe][L] - k_7[Fe][FeL] \quad (B6)$$

Thus

$$[FeL] = (k_2/k_7)[L] \quad (B7)$$

The rate expression (eq B2) is thus

$$\text{rate} = k_3(k_2/k_7)[L][Fe_2] \quad (B8)$$

The derivation of the rate expression becomes more complicated if the following step is added to the pathway.

$$Fe_2^- \xrightarrow{k_6} Fe + Fe^- \quad (B9)$$

However, as this step increases in importance, Scheme I applies. Thus, as the rate of (B9) increases relative to the k_4 step, the kinetics will shift from second-order overall (and first-order in [L]) to $^3/_2$-order overall (and half-order in [L], eq A10).

Derivation of Eq 20. The pathway is shown below.

$$Fe_2 \underset{k_{-1}}{\overset{k_1}{\rightleftharpoons}} 2Fe$$

$$Fe + L \xrightarrow{k_2} FeL + CO$$

$$FeL + Fe_2 \xrightarrow{k_3} FeL^+ + Fe_2^-$$

$$Fe_2^- + L \xrightarrow{k_6} Fe_2L^-$$

$$Fe_2L^- + Fe_2 \xrightarrow{k_7} Fe_2L + Fe_2^-$$

$$Fe_2^- \xrightarrow{k_4} Fe^- + Fe$$

$$FeL + Fe \xrightarrow{k_5} FeL^+ + Fe^-$$

Because the chain is long, the rate is

$$\text{rate} = k_7[Fe_2][Fe_2L^-] = k_6[Fe_2^-][L] \quad (C1)$$

The steady-state approximations on $[Fe_2L]$ and $[Fe_2^-]$ yield

$$\frac{d[Fe_2L^-]}{dt} = 0 = k_6[Fe_2^-][L] - k_7[Fe_2L^-][Fe_2] \quad (C2)$$

and

$$\frac{d[Fe_2^-]}{dt} = 0 = k_3[FeL][Fe_2] - k_6[Fe_2^-][L] + k_7[Fe_2L^-][Fe_2] - k_4[Fe_2^-] \quad (C3)$$

Adding (C2) and (C3) yields

$$k_3[FeL][Fe_2] = k_4[Fe_2^-] \quad (C4)$$

(This equation also follows because the rate of initiation equals the rate of termination.) or

$$(k_3/k_4)[FeL][Fe_2] = [Fe_2^-] \quad (C5)$$

Substituting (C5) into the rate expression yields

$$\text{rate} = k_6[L]\{(k_3/k_4)[FeL][Fe_2]\} \quad (C6)$$

To find [FeL], again use the steady-state approximation:

$$\frac{d[FeL]}{dt} = 0 = k_2[Fe][L] - k_3[Fe_2][FeL] - k_5[FeL][Fe] \quad (C7)$$

Therefore

$$[FeL] = \frac{k_2[Fe][L]}{k_3[Fe_2] + k_5[Fe]} \quad (C8)$$

If $k_5[Fe] \gg k_3[Fe_2]$, then

$$[FeL] = (k_2/k_5)[L] \quad (C9)$$

Substituting this equation into the rate expression (eq C6) yields

$$\text{rate} = k_6[L](k_3/k_4)[Fe_2](k_2/k_5)[L] \quad (C10)$$

or

$$\text{rate} = k'[L]^2[Fe_2] \quad (C11)$$

where $k' = k_2k_3k_6/k_4k_5$. If $k_5[Fe] \ll k_3[Fe_2]$, then eq C8 becomes

$$[FeL] = \frac{k_2[Fe][L]}{k_3[Fe_2]} \quad (C12)$$

It is now necessary to find [Fe]. The steady-state approximation on [Fe] yields

$$\frac{d[Fe]}{dt} = 0 = 2k_1[Fe_2] - 2k_{-1}[Fe]^2 - k_2[Fe][L] + k_4[Fe_2^-] - k_5[Fe][FeL] \quad (C13)$$

Adding (C13) and (C8) yields

$$0 = 2k_1[Fe_2] - 2k_{-1}[Fe]^2 - k_3[Fe_2][FeL] + k_4[Fe_2^-) - 2k_5[Fe][FeL] \quad (C14)$$

Equation C4 shows that $k_3[Fe_2][FeL] = k_4[Fe_2^-]$. Therefore

$$0 = -k[Fe_2] + k_{-1}[Fe]^2 + k_5[Fe][FeL] \quad (C15)$$

Substituting (C12) in C(15) yields

$$0 = -k_1[Fe_2] + k_{-1}[Fe]^2 + \frac{k_2k_5[L][Fe]^2}{k_3[Fe_2]} \quad (C16)$$

Thus

$$\left[\frac{k_1[Fe_2]}{k_{-1} + \dfrac{k_2k_5[L]}{k_3[Fe_2]}}\right]^{1/2} = [Fe] \quad (C17)$$

Using (C17) and (C12) in the rate expression (eq C1) yields

$$\text{rate} = \frac{k_1k_6}{k_4}[L]^2\left[\frac{k_1[Fe_2]^2}{k_{-1}[Fe_2] + \dfrac{k_2k_5}{k_3}}\right] \quad (C18)$$

If $k_{-1}[Fe_2] \gg (k_2k_5/k_3)[L]$, then

$$\text{rate} = (k_1k_6/k_4)(k_1/k_{-1})^{1/2}[L]^2[Fe_2]^{1/2} \quad (C19)$$

If $(k_2k_5/k_3)[L] \gg k_{-1}[Fe_2]$, then

$$\text{rate} = (k_1k_6/k_4)(k_1k_3/k_2k_5)^{1/2}[L]^{3/2}[Fe_2] \quad (C20)$$

Registry No. dppe, 1663-45-2; $Cp_2Fe_2(CO)_4$, 12154-95-9.

Supplementary Material Available: Two more figures from the GIT program output comparing the calculated concentration vs time curves with the experimental data for the reaction of $Cp_2Fe_2(CO)_4$ with dppe (2 pages). Ordering information is given on any current masthead page.